NANO LETTERS

pubs.acs.org/NanoLett

Letter

Engineering Biomimetic Nanostructured "Melanosome" Textiles for Advanced Solar-to-Thermal Devices

Peng Xiao, Weiqing Yang, Nianxiang Qiu, Shan Li, Feng Ni, Chang Zhang, Jincui Gu, Shiao-Wei Kuo, and Tao Chen*

Cite This: *Nano Lett.* 2022, 22, 9343−9350

Read Online

ACCESS | Metrics & More | Article Recommendations | Supporting Information

ABSTRACT: In nature, deep-sea fish featured with close-packed melanosomes can remarkably lower light reflection, which have inspired us to design ultrablack coatings for enhanced solar-to-thermal conversion. Herein, a biomimetic ultrablack textile is developed enabled by the formation of hierarchical polypyrrole (Ppy) nanospheres. The fabricated textile exhibits prominently suppressed reflectance of lower than 4% and highly enhanced absorption of up to 96%. Further experimental results and molecular dynamics (MD) simulation evidence the formation process of hierarchical nanospheres. Based on high-efficient solar-to-thermal conversion, the biomimetic textile with desirable conductivity allows the development of a salt-free solar evaporator, enabling a sustainable seawater evaporation rate of up to 1.54 kg m^{-2} h^{-1} under 1 sun. Furthermore, the biomimetic hierarchical textile exhibits good superhydrophobicity, enhanced photothermal property, and high electrothermal conversion, demonstrating significant potential in wearable thermal management (rescue vests) in water conditions.

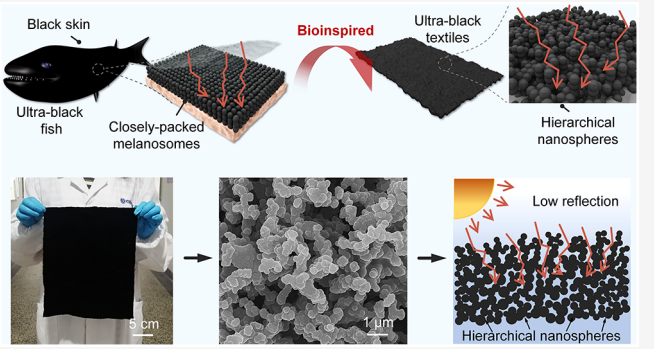

KEYWORDS: *biomimetic ultrablack textile, melanosome-like hierarchical nanospheres, solar-to-thermal conversion, solar vaporization, superhydrophobic thermal management*

Solar-to-thermal conversion is a direct and efficient way to convert incident light into considerable heat for diverse energy management and utilization.[1−11] To achieve a desirable photothermal property, extensive efforts have been dedicated to develop a diverse intrinsic materials system for sunlight capture and conversion.[8,12−18] Furthermore, combined with the design of hierarchically textured surfaces or controllable three-dimensional (3D) porous structures, significant advances have been made to suppress the reflection and enhance light absorption.[1,2,8,15,16,19−21] A typical example of MXene nanocoatings with hierarchical surface textures via the thermal shrinkage method can demonstrate light reflection lower than that of the planar one.[6] Another example of fabricating freeze-drying graphene aerogels is considered to be an efficient light capture method to remarkably extend the incidence path and increase multiple reflections.[15] In addition to the materials employed, a common characteristic of the conventional photothermal system is severely affected by the exposed water environment, which can suffer from fluctuation or severely weakened solar-to-thermal conversion performance. Based on these issues, creating water-repellent and high-efficient solar-to-thermal materials in a facile and effective way is highly desired and still remains a challenge.

In nature, there are diverse examples of black surfaces that can be used to maintain temperature, hunt, or camouflage.[22,23] For example, the polar bear has black skin underneath the white hair to efficiently absorb sunlight for maintaining body temperature.[22] In the deep sea, some fish species have evolved ultrablack skins with close-packed melanosomes to enhance the light absorption, extremely lower reflectance, and camouflage themselves for near-stealth behavior.[23]

The evolution of close-packed melanosome layers has inspired the design of synthetic ultrablack materials with a rational combination of superhydrophobic and photothermal features. Here, we have designed biomimetic melanosome-like hierarchical nanosphere layers composed of polypyrrole (Ppy) and perfluorodecyl triethoxysilane (PFTS) on a textile surface via inverse polymerization. Molecular dynamics (MD) simulations further evidenced the formation mechanism of these nanospheres. The achieved biomimetic hierarchical

Received: August 5, 2022
Revised: November 7, 2022
Published: November 15, 2022

https://doi.org/10.1021/acs.nanolett.2c02385
Nano Lett. 2022, 22, 9343−9350

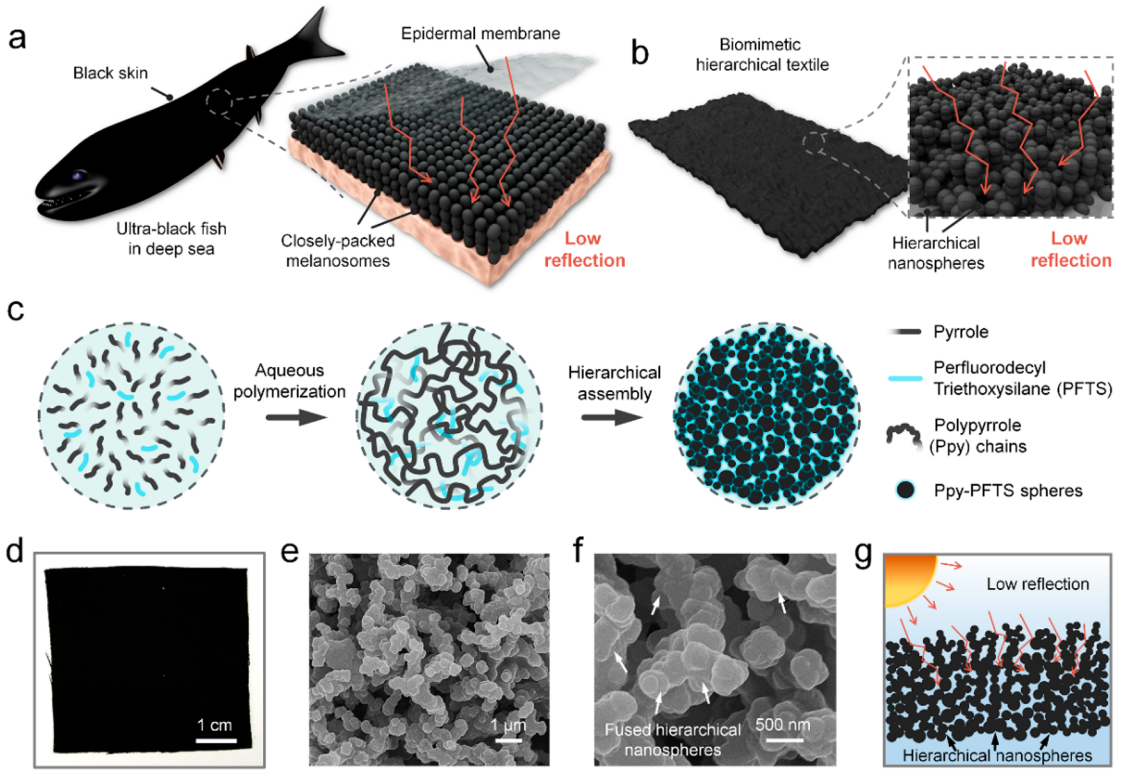

Figure 1. (a) Schematic of the ultrablack fish living in deep seawater with color camouflage via unique black skin composed of closely packed melanosomes. (b) Demonstration of synthesized bio-inspired ultrablack textile equipped with hierarchical nanospheres for enhanced light capture. (c) Schematic illustration of the formation of superhydrophobic hierarchical polypyrrole (Ppy) nanospheres. (d) Photo of Ppy-based textile, demonstrating an ultrablack color. (e,f) Scanning electron microscopy images of the hierarchical nanospheres on a textile surface. (g) Potential mechanism of light capture by the hierarchical structures.

textile exhibited superhydrophobic, conductive, and highly enhanced photothermal features with low reflection and high light absorption. Based on this desirable performance, the biomimetic hierarchical textile can function as a salt-free solar evaporator to realize stable simulated seawater evaporation. Moreover, the textile can be further applied as a superhydrophobic thermal management device enabled by solar energy under extreme environments.[24,25] When exposed or treated by water, it can still maintain a continuous and stable surface temperature for advanced rescue vests, demonstrating significant potentials in multifunctional solar-to-thermal applications.

Some deep sea fish featuring ellipsoid-like densely packed melanosomes can camouflage themselves with ultrablack skins to effectively reduce the light reflectance and increase the light path length and absorption (Figure 1a).[23] Here, the close-packed melanosomes were imitated, and hierarchical Ppy nanospheres grown on the textile surface were constructed in our system (Figure 1b). The fabrication strategy was based on a wet method, of which the mixture of pyrrole and PFTS on the textile was immersed into water solution containing the initiator $FeCl_3$. Followed by a typical pyrrole polymerization and PFTS hydrolytic process, the polymerized Ppy further assembled into nanospheres to achieve surface energy minimization. As the polymerized Ppy chains were composed of conjugated units, they represented a hydrophobic property. Moreover, the introduction of fluorinated additive and the resulting hydrolyzed derivatives into the Ppy system can remarkably reduce the surface energy. After hierarchical assembly of Ppy-based nanospheres, close-packed melanosome-like layers were formed on the textile (Figure 1c). As shown in Figure 1d, a homogeneous biomimetic textile was achieved. The enhanced light absorption capability was derived from the hierarchical and compacted stacking of nanoscale Ppy spheres (Figure 1e). The amplified scanning electron microscopy (SEM) image in Figure 1f can further demonstrate that the adjacent spheres have fused together for a relatively stable structure. Furthermore, there exist some nanoscale gaps inside the synthetic melanosome layers, allowing the effective capture of incident light via high scattering and multiple inner reflection (Figure 1g).

The close-packed nanosphere coating is expected to be an effective strategy to maximize the efficiency of incident light capture. Based on this, as schematically illustrated in Figure 2a, compared with the laminated structures, the Ppy nanospheres are considered to induce multiple light scattering and internal reflections inside the hierarchical structures. Since the laminated structure was formed by putting the $FeCl_3$ interacting textile into the pyrrole/chloroform solution, the formed hydrophobic Ppy chains could be effectively wetted by the solution for stretching conformation. As a result, the laminated Ppy morphology was finally formed (Figure 2b).[17,26] From the SEM image in Figure 2c, it can be clearly observed that there are closely packed nanospheres and relatively uniform gaps on the textile surface, ensuring low reflectance performance of the biomimetic textile. UV−vis−IR spectra further illustrated that the hierarchical Ppy nanospheres presented lower transmittance and reflectance (reflectance value was lower than 0.8% within the visible light area) almost over the whole wavelength range compared to that of

https://doi.org/10.1021/acs.nanolett.2c02385
Nano Lett. 2022, 22, 9343−9350

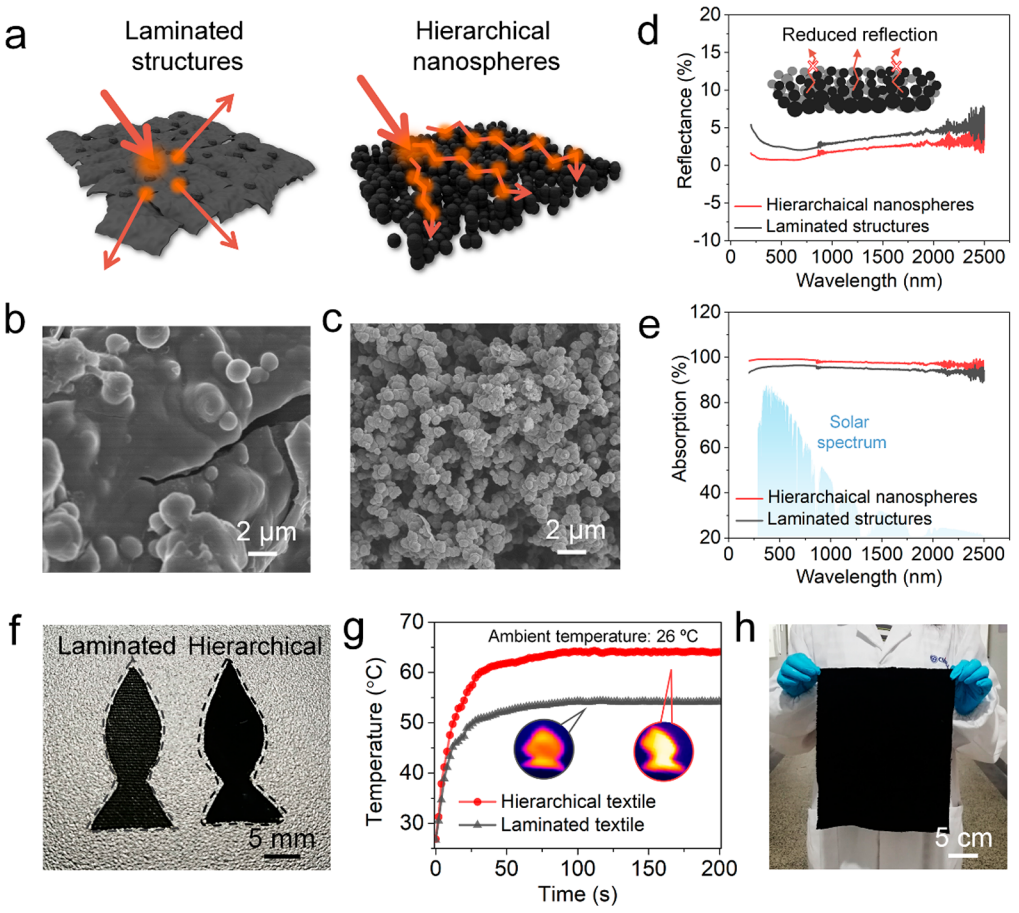

Figure 2. (a) Schematic illustration of a laminated Ppy layer and biomimetic sphere-like Ppy layer, demonstrating enhanced light capture performance of the biomimetic structure. (b,c) SEM images of laminated Ppy structures and hierarchical Ppy nanospheres. (d,e) UV−vis−IR spectra of laminated and sphere-like Ppy layers: reflectance spectrum and absorption spectrum, showing enhanced light capture capability of the hierarchical Ppy spheres layer with lower reflectance and higher absorption. (f) Photo of fish-shaped Ppy-based textile of laminated and hierarchical structures with enhanced blackness. (g) Corresponding temperature versus time curves under 1 sun illumination. (h) Photo of a large-scale biomimetic sphere-like Ppy-based textile.

laminated structures (Figure 2d and Figure S1). In addition, the total light absorption performance (the absorption value could reach up to over 99% within the visible light area) of the biomimetic structure was higher than that of the laminated one (Figure 2e and Figure S2). Moreover, the surface roughness of the hierarchical textile (R_a ~3.0 μm) was remarkably larger than that of the laminated one (R_a ~1.5 μm), enabling the transmittance to be enhanced and depressing the reflectance (Figure S3). Moreover, for the universality of the targeted substrates, nanofiber-enabled nonwoven fabric modified with hierarchical Ppy nanospheres was also fabricated, showing a light absorption relatively lower than that of the biomimetic textile (Figure S4).

Macroscopically, the biomimetic textile showed a color much darker than that of the laminated one in natural light (Figure 2f). Furthermore, Figure 2g clearly showed that the equilibrium solar-to-thermal conversion temperature of the hierarchical and laminated textile presented the values of ~65 and ~55 °C, respectively, under 1 sun illumination. Also, the mechanical abrasion resistance of the biomimetic textile was also considered. Benefitting from the fused connection between nanospheres, the hierarchical nanosphere-enabled surface represented favorable mechanical stability under rigorous abrasive paper (P600) with 500 g weight applied (Figure S5a,b). Note that even if the outermost Ppy layer is damaged, the next layer can still present good superhydrophobic features (Figure S5c,d). Moreover, the hierarchical textile also demonstrated good mechanical strength for further wearable applications (Figure S6). Based on the facile, efficient, and scalable strategy, a large-area biomimetic textile was constructed in Figure 2h and Figure S7.

To investigate the formation mechanism of hierarchical nanosphere structures, the process of structural formation was carefully investigated through SEM images. As shown in Figures S8−S10, prior to the formation of Ppy nanospheres, a homogeneous Ppy coating was first formed on the of textile surface. Following the continuous increase of nanospheres, the hierarchical Ppy nanospheres fully covered the textile for close-packed nanostructures, demonstrating a structural advantage of formation of superhydrophobic surfaces.[27−29] Owing to the introduction of hydrophobic PFTS, the hierarchically nanostructured surface represented superhydrophobic wettability with water contact angle (WCA) values of 159 and 156°, respectively, on the front and back side (Figure S11). Moreover, energy-dispersive spectrometry (EDS) showed that there was uniform distribution of the characteristic N from Ppy chains and the F from hydrolyzed PFTS chains (Figure S12−S14). X-ray photoelectron spectroscopy (XPS) measurement further demonstrated that the outermost layer of the hierarchical textile contained F with a content greater than

https://doi.org/10.1021/acs.nanolett.2c02385
Nano Lett. 2022, 22, 9343−9350

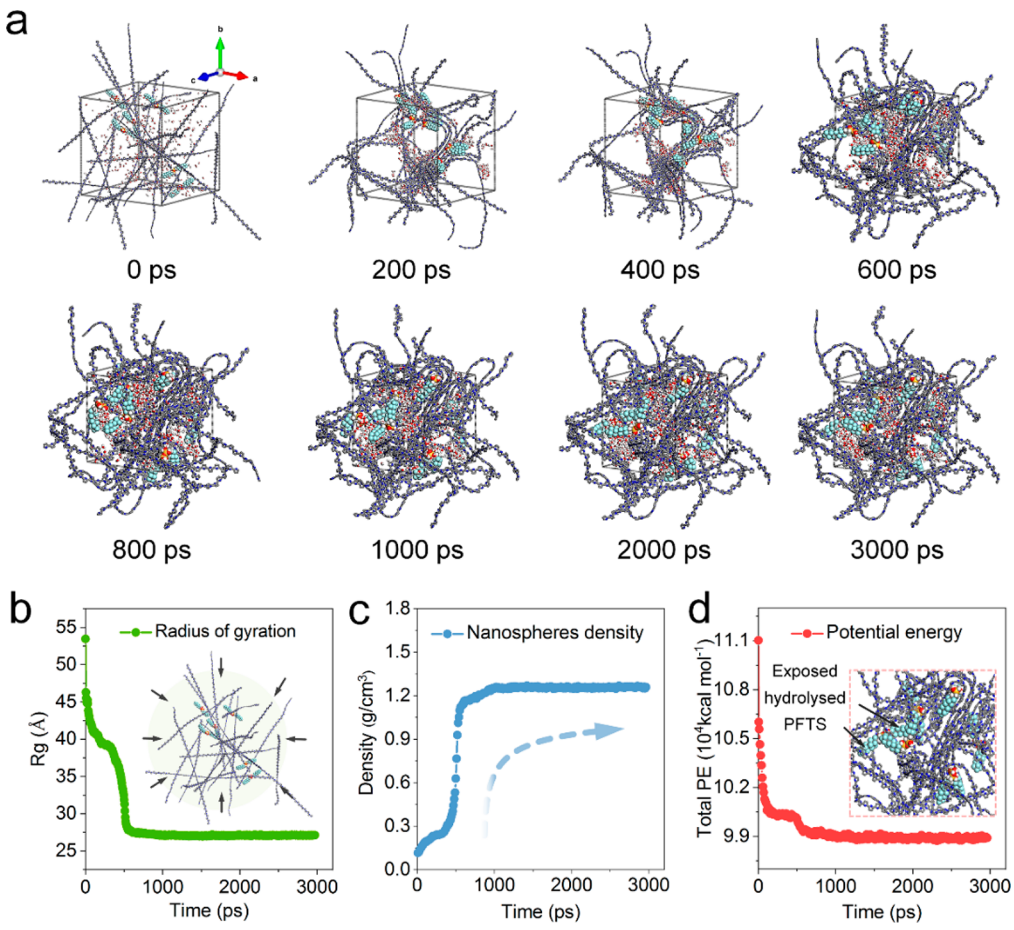

Figure 3. (a) MD simulation for the formation process of nanospheres within 3000 ps. (b) R_g value of nanosphere versus time curve with a decrease trend. Inset: Original Ppy and hydrolyzed PFTS chains randomly distributed in the unit. (c) Density of nanosphere versus time curve, representing a gradual increased value. (d) Total potential energy of the whole system versus time curve, which decreases and tends to be a balanced state. Inset: Amplified model of the nanosphere, demonstrating the hydrolyzed PFTS partially exposed to the air.

50%, enabling the improvement of the water-repellent performance (Figure S15).

The potential mechanism of the melanosome-like hierarchical nanospheres was further explored through MD simulations using the Materials Studio software, and the COMPASS force field was employed to determine the interactions between atoms. As shown in Figure 3a and Figure S16, polymerized Ppy chains and hydrolyzed PFTS were homogeneously distributed in the bulk water solution. Since the Ppy chains and hydrolyzed PFTS are hydrophobic and incompatible with the bulk water phase, they tended to adjust their conformation into a sphere-like collapsed state. The exposed PFTS chains are expected to remarkably decrease the surface energy. Moreover, the radius of gyration (R_g) during the formation of nanospheres was calculated in the simulation experiments. As displayed in Figure 3b, with the increase of time, the value of R_g experienced a decreasing trend from 53.46 to 27.14 Å. In addition, the density of the nanospheres was also estimated, resulting in a remarkable increase from 0.12 to 1.26 g/cm^3 (Figure 3c). Furthermore, we calculated the potential energy of the whole system in the process of nanosphere formation. Figure 3d clearly shows that the potential energy exhibited a gradual decrease tendency from 11.10×10^4 to 9.89×10^4 kcal mol^{-1}. More importantly, from the amplified image in Figure 3d, it could be observed that the hydrolyzed PFTS was partially exposed to the outer surface of the Ppy nanospheres, providing low surface energy to the whole system.

Benefitting from the effective combination of enhanced photothermal conversion and superhydrophobicity, a contactless infrared (IR) irradiation mode can be employed to heat the water, which can exhibit significant potentials in sustainable salt-free seawater evaporation.[13,30] As displayed in Figure 4a, the biomimetic textile was combined with hydrophilic cotton textiles to construct integrated solar/electricity-enabled evaporators for solar and/or Joule heating. Note that the generated high temperature (65 °C under 1 sun) could indirectly heat the water molecules via a contactless IR irradiation strategy, enabling efficient and sustainable water evaporation without salt contamination.[31] As displayed in Figure 4b,c, the evaporation rate of pure water and simulated seawater (3.5 wt % NaCl) could reach up to relatively high values of 1.65 and 1.54 kg m^{-2} h^{-1}, respectively, under 1 sun. In addition, the resultant evaporation rate in 5, 10, and 20 wt % NaCl solution represented 1.40, 1.21, and 1.05 kg m^{-2} h^{-1}, individually. The corresponding solar vaporization efficiencies were also calculated under different circumstances, demonstrating a decreased tendency due to the increase of salt content (Figure S17).

Also, the laminated textile and the hierarchical one were employed to conduct the long-time continuous evaporation experiments with 3.5 wt % NaCl solution. 2D IR images clearly

https://doi.org/10.1021/acs.nanolett.2c02385
Nano Lett. 2022, 22, 9343−9350

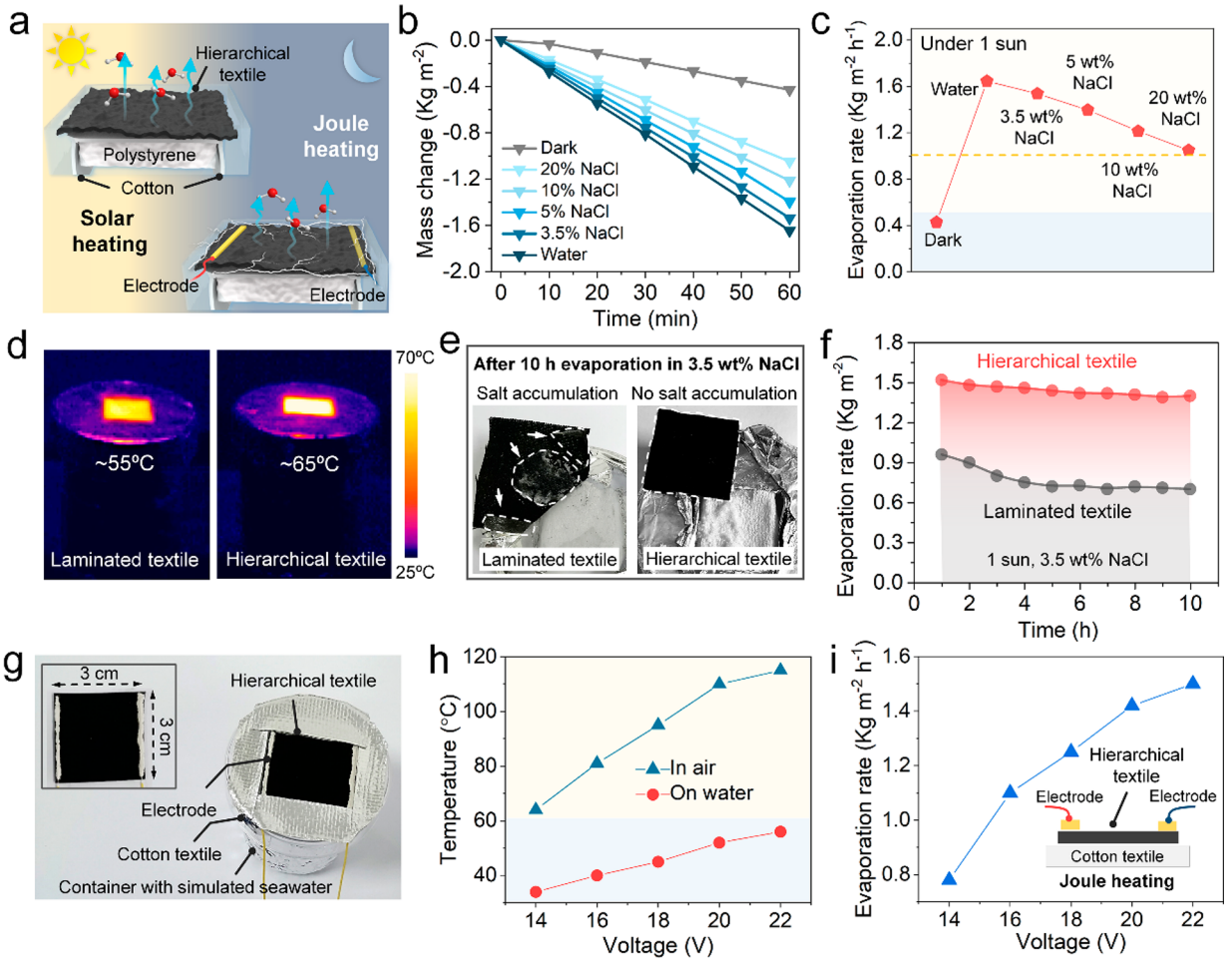

Figure 4. (a) Sketch of the textile-based solar/electricity evaporators composed of hydrophilic cotton and superhydrophobic photothermal textile for solar heating and Joule heating. (b) Mass change curves of the evaporator conducted in water and simulated seawater with different concentration from 3.5 to 20 wt %. (c) Evaporation rates of a series of liquids. (d) 2D IR images of the laminated and hierarchical textiles under 1 sun illumination. (e) Photos of the textile after 10 h evaporation in 3.5 wt % NaCl under 1 sun. (f) Long-time continuous evaporation rates of the laminated and hierarchical fabric in 3.5 wt % simulated seawater. (g) Photo of the Joule heating-enabled evaporator floated on the water surface. (h) Temperature versus applied voltage curves in air and on the water surface. (i) Evaporation rates under a series of applied voltages.

illustrated that the hierarchical textile-based evaporator represented temperatures higher that those of the laminated ones (Figure 4d). After 10 h continuous evaporation under 1 sun, there was a visible aggregate of NaCl particles on the surface of the laminated textile. However, no remarkable salt accumulation can be observed on the hierarchical textile (Figure 4e). The evaporation rate of the laminated textile-based evaporator severely reduced to 0.72 kg m^{-2} h^{-1} after 4 h. In contrast, the hierarchical textile-based evaporator still maintained a stable evaporation rate from 1.52 to 1.4 kg m^{-2} h^{-1} (Figure 4f).

Owing to the conjugated structural units of Ppy chains, the macroscopically assembled fused nanopheres also exhibit good conductivity.[32] To construct the Joule heating-based evaporator,[33,34] Ag paste with a wire was first coated on the hierarchical textile surface for conformal spreading. After curing, the interfacial contact resistance could be significantly decreased, ensuring favorable electrothermal conversion for seawater evaporation in the absence of sunlight (Figure 4g). As shown in Figure 4h, the biomimetic textiles reached an equilibrium temperature of 64, 81, 95, 110, and 115 °C under voltages of 14, 16, 18, 20, and 22 V, respectively. Based on the Joule heating mechanism, the electric-heating-enabled evaporation rates can be effectively adjusted ranging from 0.78 to 1.5 kg m^{-2} h^{-1} under the applied voltage from 14 to 22 V (Figure 4i).

More interestingly, the biomimetic textile featured with favorable photothermal and superhydrophobic properties can be further employed to realize solar-enabled thermal management.[6,35] As displayed in Figure 5a, Ppy-based textiles with laminated and hierarchical structures were cut into photothermal vests. Superior to the laminated structure, the hierarchical one exhibited a higher temperature of ~72.7 °C under 1 sun (Figure 5b). Even weak solar intensity of 0.4 sun can still result in the equilibrium temperature of 47.7 °C of the biomimetic hierarchical textile (Figure 5c). Note that for the wearable textile, the generated high temperature has the risk of ambustion. However, the air layer between textile and body skin can effectively avoid the risk. Furthermore, the contactless IR irradiation heating strategy through the air medium could provide considerable thermal energy under safe circumstances.[35] When exposed to the water-related condition, the biomimetic textile could effectively repel water droplets, enabling an obvious bouncing phenomenon formed (Figure 5d). As shown in Figure 5e, there was remarkable water residue observed on the surface of the laminated textile, which may

https://doi.org/10.1021/acs.nanolett.2c02385
Nano Lett. 2022, 22, 9343−9350

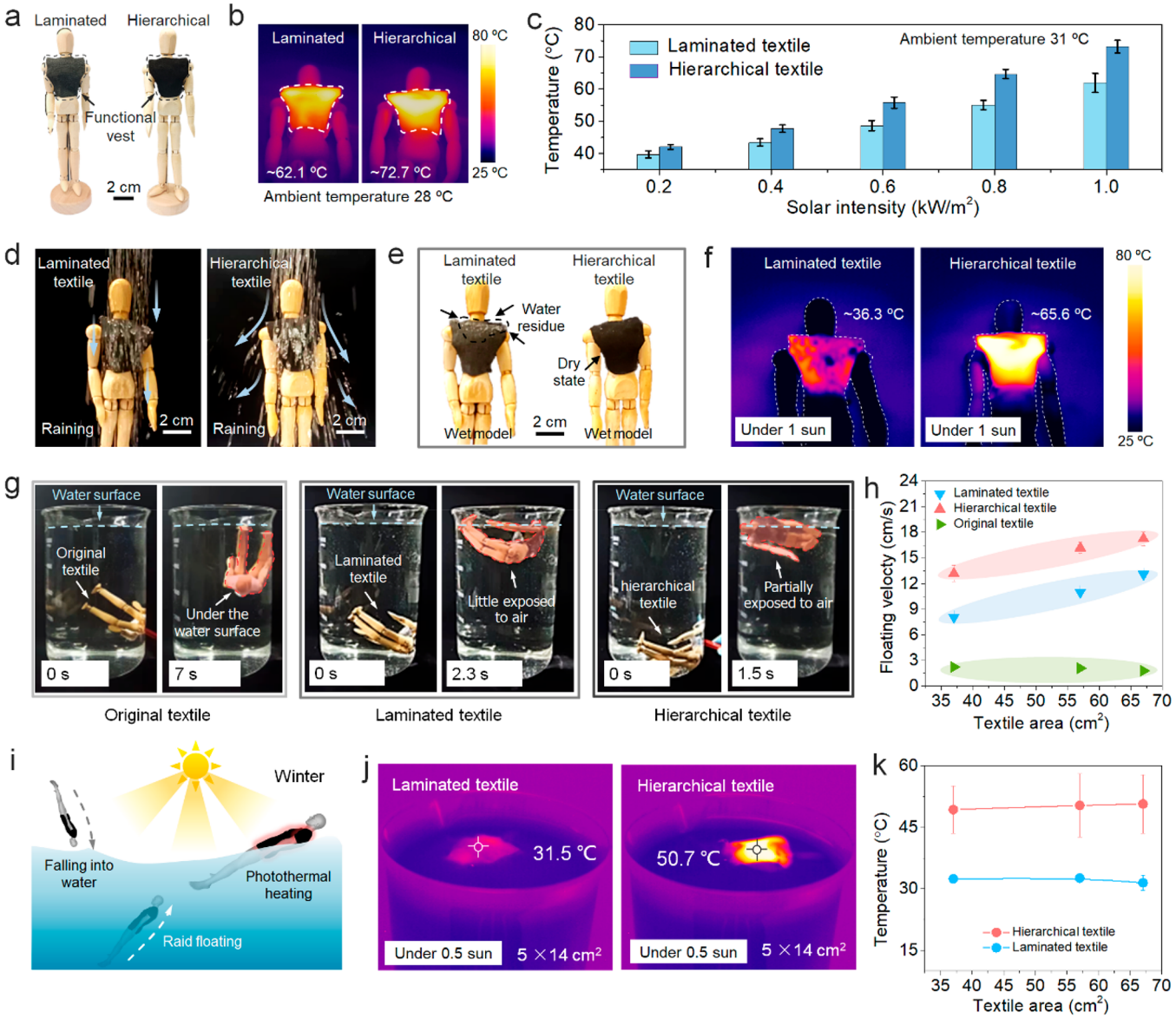

Figure 5. (a) Photo of the hierarchical Ppy textile-based vest and the laminated one on human models. (b) Corresponding 2D IR image of laminated and hierarchical Ppy textile. (c) Temperature versus solar intensity columns of hierarchical and laminated textiles. (d–f) Photos and IR image of the two styles of textile after treated by simulated rain. (g) Photos of the demonstration of an underwater rescue vest enabled by original, laminated, and hierarchical textiles. (h) Rising velocity versus textile area of the aforementioned three samples. (i) Sketch illustration of the biomimetic textile enabled rescue vest, which can provide considerable buoyancy and further generate stable and sustainable heat under sunlight not affected by the water environment. (j) Corresponding temperature of laminated and hierarchical rescue vest under 0.5 sun when floated on a water surface. (k) Temperature versus textile area curves of laminated and hierarchical textile.

severely decrease the surface temperature, resulting in a surface temperature from 62.1 to 36.3 °C under 1 sun. However, the biomimetic textile could still maintain a relatively stable temperature of 65.6 °C under 1 sun (Figure 5f). For the wearable textile, air permeability and water vapor transmission are also important for a comfortable experience. Due to the hierarchical structure with abundant pores, the hierarchical textile only exhibited good air/water permeability (Figure S18).

Benefitting from the superhydrophobic feature of the hierarchical textile, a demonstration of water rescue was demonstrated in Figure 5g. When a person falls into the water from the boat on a sunny winter day, the cold water can severely lower their body temperature, freeze the body, and further limit the body behavior. As shown in Figure 5g, the human model with blank textiles is still located under the water surface due to the weak buoyancy. Superior to the laminated textile, most of the hierarchical one was exposed to the air due to its superhydrophobic feature. More importantly, a series of vest areas were further adopted to investigate the relationship between the textile area and floating velocity (Figure S19). As a result, the rescue vest with a hierarchical textile could reach the highest velocity of ~ 17.3 cm/s with a fabric area of ~67 cm^2, whereas the laminated one demonstrated a velocity of ~13.1 cm/s with the same textile area (Figure 5h). As a demonstration, the biomimetic hierarchical textile could provide extra buoyancy for remarkably enhanced floating velocity and effectively remain warm under sunlight irradiation (Figure 5i). As illustrated in Figure 5j, superior to the laminated textile at ~31.5 °C under 0.5 sun, the hierarchical

https://doi.org/10.1021/acs.nanolett.2c02385
Nano Lett. 2022, 22, 9343−9350

one demonstrated a favorable temperature of ∼50.7 °C even with low solar intensity. Moreover, the equilibrium temperature of the vest with a series of textile areas could still maintain a stable value (Figure 5k).

In summary, a bio-inspired ultrablack textile featured with enhanced photothermal and favorable superhydrophobic properties is rationally designed to achieve enhanced and water-resistant solar-to-thermal conversion applications. The favorable characteristic can derive from the formation of hierarchical nanospheres with low surface energy on textile surfaces. The achieved superhydrophobic photothermal textile can function as a contactless solar/electrical-enabled evaporator for salt-free and efficient seawater evaporation. Furthermore, it can be further integrated into a wearable solar-to-thermal rescue vest to realize underwater rescue and maintain sustainable solar-enabled thermal supply. The design principle of the superhydrophobic photothermal textile is expected to provide a pathway for advanced solar-to-thermal conversion devices, such as sustainable seawater desalination, water-resistant solar heating devices, efficient photothermal actuators on water, etc.

■ ASSOCIATED CONTENT

Supporting Information

The Supporting Information is available free of charge at https://pubs.acs.org/doi/10.1021/acs.nanolett.2c02385.

Transmittance, reflection and absorption curves of the laminated and hierarchical textiles (Figures S1 and S2); Surface roughness of the hierarchical textile (Figure S3); SEM images and light absorption of the hierarchical nanofibers (Figure S4); friction measurement and corresponding WCA values of the hierarchical textile (Figure S5); mechanical strength of the textile (Figure S6); photo of hierarchical textile with favorable superhydrophobic feature (Figure S7); schematic illustration and SEM surface and cross-sectional images of the forming process of the hierarchical textiles (Figures S8, S9, and S10); WCA characterization of the textile (Figure S11); EDS mapping and quantitative distribution of certain elements on hierarchical textile (Figures S12−S14); XPS characterization of the hierarchical textile (Figure S15); chemical structures employed in the molecular simulation process (Figure S16); solar vaporization efficiencies (Figure S17); air permeability and water vapor transmission (Figure S18); photos of photothermal vests with a series of sizes fabricated by laminated and hierarchical textiles (Figure S19) (PDF)

■ AUTHOR INFORMATION

Corresponding Author

Tao Chen − *Key Laboratory of Marine Materials and Related Technologies, Zhejiang Key Laboratory of Marine Materials and Protective Technologies, Ningbo Institute of Materials Technology and Engineering, Chinese Academy of Sciences, Ningbo 315201, China; School of Chemical Sciences, University of Chinese Academy of Sciences, Beijing 100049, China;* orcid.org/0000-0001-9704-9545; Email: tao.chen@nimte.ac.cn

Authors

Peng Xiao − *Key Laboratory of Marine Materials and Related Technologies, Zhejiang Key Laboratory of Marine Materials and Protective Technologies, Ningbo Institute of Materials Technology and Engineering, Chinese Academy of Sciences, Ningbo 315201, China; School of Chemical Sciences, University of Chinese Academy of Sciences, Beijing 100049, China;* orcid.org/0000-0003-2231-9824

Weiqing Yang − *Key Laboratory of Marine Materials and Related Technologies, Zhejiang Key Laboratory of Marine Materials and Protective Technologies, Ningbo Institute of Materials Technology and Engineering, Chinese Academy of Sciences, Ningbo 315201, China; School of Chemical Sciences, University of Chinese Academy of Sciences, Beijing 100049, China*

Nianxiang Qiu − *Key Laboratory of Marine Materials and Related Technologies, Zhejiang Key Laboratory of Marine Materials and Protective Technologies, Ningbo Institute of Materials Technology and Engineering, Chinese Academy of Sciences, Ningbo 315201, China; School of Chemical Sciences, University of Chinese Academy of Sciences, Beijing 100049, China*

Shan Li − *Key Laboratory of Marine Materials and Related Technologies, Zhejiang Key Laboratory of Marine Materials and Protective Technologies, Ningbo Institute of Materials Technology and Engineering, Chinese Academy of Sciences, Ningbo 315201, China; School of Chemical Sciences, University of Chinese Academy of Sciences, Beijing 100049, China*

Feng Ni − *Key Laboratory of Marine Materials and Related Technologies, Zhejiang Key Laboratory of Marine Materials and Protective Technologies, Ningbo Institute of Materials Technology and Engineering, Chinese Academy of Sciences, Ningbo 315201, China; School of Chemical Sciences, University of Chinese Academy of Sciences, Beijing 100049, China*

Chang Zhang − *Key Laboratory of Marine Materials and Related Technologies, Zhejiang Key Laboratory of Marine Materials and Protective Technologies, Ningbo Institute of Materials Technology and Engineering, Chinese Academy of Sciences, Ningbo 315201, China; School of Chemical Sciences, University of Chinese Academy of Sciences, Beijing 100049, China*

Jincui Gu − *Key Laboratory of Marine Materials and Related Technologies, Zhejiang Key Laboratory of Marine Materials and Protective Technologies, Ningbo Institute of Materials Technology and Engineering, Chinese Academy of Sciences, Ningbo 315201, China; School of Chemical Sciences, University of Chinese Academy of Sciences, Beijing 100049, China*

Shiao-Wei Kuo − *Department of Material and Optoelectronic Science, Center of Crystal Research, National Sun Yat-Sen University, Kaohsiung 804, Taiwan;* orcid.org/0000-0002-4306-7171

Complete contact information is available at: https://pubs.acs.org/10.1021/acs.nanolett.2c02385

Notes

The authors declare no competing financial interest.

■ ACKNOWLEDGMENTS

This research was supported by the Natural Science Foundation of China (52073295), Ningbo Science and Technology Bureau (2021Z127), the Sino-German Mobility Program (M-0424), Ningbo Public Welfare Science and

Technology Plan Project (2021S150), Key Research Program of Frontier Sciences, Chinese Academy of Sciences (QYZDB-SSWSLH036), Bureau of International Cooperation, Chinese Academy of Sciences (174433KYSB20170061), and K.C. Wong Education Foundation (GJTD-2019-13).

REFERENCES

(1) Zhou, L.; Tan, Y.; Ji, D.; Zhu, B.; Zhang, P.; Xu, J.; Gan, Q.; Yu, Z.; Zhu, J. Self-assembly of highly efficient, broadband plasmonic absorbers for solar steam generation. *Sci. Adv.* **2016**, *2*, No. e1501227.
(2) Wang, X.; Liu, Q. C.; Wu, S. Y.; Xu, B. X.; Xu, H. X. Multilayer Polypyrrole Nanosheets with Self-Organized Surface Structures for Flexible and Efficient Solar-Thermal Energy Conversion. *Adv. Mater.* **2019**, *31*, 1807716.
(3) Lyu, S.; He, Y.; Yao, Y.; Zhang, M.; Wang, Y. Photothermal Clothing for Thermally Preserving Pipeline Transportation of Crude Oil. *Adv. Funct. Mater.* **2019**, *29*, 1900703.
(4) Han, B.; Zhang, Y. L.; Chen, Q. D.; Sun, H. B. *Carbon-Based Photothermal Actuators. Adv. Funct. Mater.* **2018**, *28*, 1802235.
(5) Zhu, L. L.; Ding, T. P.; Gao, M. M.; Peh, C. K. N.; Ho, G. W. Shape Conformal and Thermal Insulative Organic Solar Absorber Sponge for Photothermal Water Evaporation and Thermoelectric Power Generation. *Adv. Energy Mater.* **2019**, *9*, 1900250.
(6) Li, K.; Chang, T.-H.; Li, Z.; Yang, H.; Fu, F.; Li, T.; Ho, J. S.; Chen, P.-Y. Biomimetic MXene Textures with Enhanced Light-to-Heat Conversion for Solar Steam Generation and Wearable Thermal Management. *Adv. Energy Mater.* **2019**, *9*, 1901687.
(7) Xiao, P.; He, J.; Ni, F.; Zhang, C.; Liang, Y.; Zhou, W.; Gu, J.; Xia, J.; Kuo, S.-W.; Chen, T. Exploring interface confined water flow and evaporation enables solar-thermal-electro integration towards clean water and electricity harvest via asymmetric functionalization strategy. *Nano Energy* **2020**, *68*, 104385.
(8) Lin, K.-T.; Lin, H.; Yang, T.; Jia, B. Structured graphene metamaterial selective absorbers for high efficiency and omnidirectional solar thermal energy conversion. *Nat. Commun.* **2020**, *11*, 1389.
(9) Lewis, N. S. Research opportunities to advance solar energy utilization. *Science* **2016**, *351*, aad1920.
(10) Wang, X.-Q.; Tan, C. F.; Chan, K. H.; Xu, K.; Hong, M.; Kim, S.-W.; Ho, G. W. Nanophotonic-Engineered Photothermal Harnessing for Waste Heat Management and Pyroelectric Generation. *ACS Nano* **2017**, *11*, 10568−10574.
(11) Ding, T.; Ho, G. W. Using the sun to co-generate electricity and freshwater. *Joule* **2021**, *5*, 1639−1641.
(12) Zhao, F.; Zhou, X.; Shi, Y.; Qian, X.; Alexander, M.; Zhao, X.; Mendez, S.; Yang, R.; Qu, L.; Yu, G. Highly efficient solar vapour generation via hierarchically nanostructured gels. *Nat. Nanotechnol.* **2018**, *13*, 489−495.
(13) Weng, D. H.; Xu, F. C.; Li, X.; Li, Y.; Sun, J. Q. Bioinspired photothermal conversion coatings with self-healing superhydrophobicity for efficient solar steam generation. *J. Mater. Chem. A* **2018**, *6*, 24441−24451.
(14) Li, W.; Li, Z.; Bertelsmann, K.; Fan, D. E. Portable Low-Pressure Solar Steaming-Collection Unisystem with Polypyrrole Origamis. *Adv. Mater.* **2019**, *31*, 1900720.
(15) Hu, X. Z.; Xu, W. C.; Zhou, L.; Tan, Y. L.; Wang, Y.; Zhu, S. N.; Zhu, J. Tailoring Graphene Oxide-Based Aerogels for Efficient Solar Steam Generation under One Sun. *Adv. Mater.* **2017**, *29*, 1604031.
(16) Peng, Y.; Zhao, W.; Ni, F.; Yu, W.; Liu, X. Forest-like Laser-Induced Graphene Film with Ultrahigh Solar Energy Utilization Efficiency. *ACS Nano* **2021**, *15*, 19490−19502.
(17) Xiao, P.; Gu, J.; Zhang, C.; Ni, F.; Liang, Y.; He, J.; Zhang, L.; Ouyang, J.; Kuo, S.-W.; Chen, T. A scalable, low-cost and robust photo-thermal fabric with tunable and programmable 2D/3D structures towards environmentally adaptable liquid/solid-medium water extraction. *Nano Energy* **2019**, *65*, 104002.
(18) Meng, S.; Zha, X.-J.; Wu, C.; Zhao, X.; Yang, M.-B.; Yang, W. Interfacial Radiation-Absorbing Hydrogel Film for Efficient Thermal Utilization on Solar Evaporator Surfaces. *Nano Lett.* **2021**, *21*, 10516−10524.
(19) Zhang, P. P.; Li, J.; Lv, L. X.; Zhao, Y.; Qu, L. T. Vertically Aligned Graphene Sheets Membrane for Highly Efficient Solar Thermal Generation of Clean Water. *ACS Nano* **2017**, *11*, 5087−5093.
(20) Ma, Q. L.; Yin, P. F.; Zhao, M. T.; Luo, Z. Y.; Huang, Y.; He, Q. Y.; Yu, Y. F.; Liu, Z. Q.; Hu, Z. N.; Chen, B.; Zhang, H. MOF-Based Hierarchical Structures for Solar-Thermal Clean Water Production. *Adv. Mater.* **2019**, *31*, 1808249.
(21) Yin, Z.; Wang, H.; Jian, M.; Li, Y.; Xia, K.; Zhang, M.; Wang, C.; Wang, Q.; Ma, M.; Zheng, Q.-s.; Zhang, Y. Extremely Black Vertically Aligned Carbon Nanotube Arrays for Solar Steam Generation. *ACS Appl. Mater. Interfaces* **2017**, *9*, 28596−28603.
(22) August, A.; Kneer, A.; Reiter, A.; Wirtz, M.; Sarsour, J.; Stegmaier, T.; Barbe, S.; Gresser, G. T.; Nestler, B. A bionic approach for heat generation and latent heat storage inspired by the polar bear. *Energy* **2019**, *168*, 1017−1030.
(23) Davis, A. L.; Thomas, K. N.; Goetz, F. E.; Robison, B. H.; Johnsen, S.; Osborn, K. J. Ultra-black Camouflage in Deep-Sea Fishes. *Curr. Biol.* **2020**, *30*, 3470.
(24) Wang, H.; Zhang, Y.; Liang, X.; Zhang, Y. Smart Fibers and Textiles for Personal Health Management. *ACS Nano* **2021**, *15*, 12497−12508.
(25) Gao, Q.; Lauster, T.; Kopera, B. A. F.; Retsch, M.; Agarwal, S.; Greiner, A. Breathable and Flexible Dual-Sided Nonwovens with Adjustable Infrared Optical Performances for Smart Textile. *Adv. Funct. Mater.* **2022**, *32*, 2108808.
(26) Ni, F.; Xiao, P.; Zhang, C.; Liang, Y.; Gu, J. C.; Zhang, L.; Chen, T. Micro-/Macroscopically Synergetic Control of Switchable 2D/3D Photothermal Water Purification Enabled by Robust, Portable, and Cost-Effective Cellulose Papers. *ACS Appl. Mater. Interfaces* **2019**, *11*, 15498−15506.
(27) Ou, J.; Wang, Z.; Wang, F.; Xue, M.; Li, W.; Amirfazli, A. Washable and antibacterial superhydrophbic fabric. *Appl. Surf. Sci.* **2016**, *364*, 81−85.
(28) Tuteja, A.; Choi, W.; Ma, M.; Mabry, J. M.; Mazzella, S. A.; Rutledge, G. C.; McKinley, G. H.; Cohen, R. E. Designing superoleophobic surfaces. *Science* **2007**, *318*, 1618−1622.
(29) Deng, X.; Mammen, L.; Butt, H.-J.; Vollmer, D. Candle Soot as a Template for a Transparent Robust Superamphiphobic Coating. *Science* **2012**, *335*, 67−70.
(30) Chen, J.; Yin, J. L.; Li, B.; Ye, Z.; Liu, D.; Ding, D.; Qian, F.; Myung, N. V.; Zhang, Q.; Yin, Y. Janus Evaporators with Self-Recovering Hydrophobicity for Salt-Rejecting Interfacial Solar Desalination. *ACS Nano* **2020**, *14*, 17419−17427.
(31) Menon, A. K.; Haechler, I.; Kaur, S.; Lubner, S.; Prasher, R. S. Enhanced solar evaporation using a photo-thermal umbrella for wastewater management. *Nat. Sustain.* **2020**, *3*, 144−151.
(32) McGrail, B. T.; Sehirlioglu, A.; Pentzer, E. Polymer Composites for Thermoelectric Applications. *Angew. Chem., Int. Ed.* **2015**, *54*, 1710−1723.
(33) He, W.; Li, G.; Zhang, S.; Wei, Y.; Wang, J.; Li, Q.; Zhang, X. Polypyrrole/Silver Coaxial Nanowire Aero-Sponges for Temperature-Independent Stress Sensing and Stress-Triggered Joule Heating. *ACS Nano* **2015**, *9*, 4244−4251.
(34) Xia, D.; Xu, Y.; Mannering, J.; Ma, X.; Ismail, M. S.; Borman, D.; Baker, D. L.; Pourkashanian, M.; Menzel, R. Tuning the Electrical and Solar Thermal Heating Efficiencies of Nanocarbon Aerogels. *Chem. Mater.* **2021**, *33*, 392−402.
(35) Shi, M.; Shen, M.; Guo, X.; Jin, X.; Cao, Y.; Yang, Y.; Wang, W.; Wang, J. Ti3C2Tx MXene-Decorated Nanoporous Polyethylene Textile for Passive and Active Personal Precision Heating. *ACS Nano* **2021**, *15*, 11396−11405.

https://doi.org/10.1021/acs.nanolett.2c02385
Nano Lett. 2022, 22, 9343−9350